Passive millimeter wave imaging sensors for commercial markets

Jonathan J. Lynch,* Perry A. Macdonald, Harris P. Moyer, and Robert G. Nagele

Microelectronics Laboratory, HRL Laboratories, LLC, 3011 Malibu Canyon Road, Malibu, California 90265, USA

*Corresponding author: jjlynch@hrl.com

Received 20 November 2009; accepted 10 March 2010; posted 16 March 2010 (Doc. ID 118896); published 7 April 2010

We describe the development of passive millimeter wave imaging sensors, operating at W band, that are currently being manufactured for commercial markets using standard automated assembly processes. A description of HRL Laboratories' millimeter wave imaging chipset is presented, focusing on parameters that limit sensor performance, such as detector $1/f$ noise, low noise amplifier noise figure, and gain drift. We conclude with a discussion of ongoing research and development in passive millimeter wave imaging and performance improvements that can be expected for future imaging sensors.

OCIS codes: 280.4991, 350.4010.

1. Introduction

For the past two decades researchers have leveraged advances in compound semiconductors to develop passive imaging sensors that operate within atmospheric absorption windows in the millimeter wave frequency band (30 to 300 GHz). At these long wavelengths electromagnetic energy penetrates materials that are opaque at shorter wavelengths. This phenomenology enables video cameras that see through fog, dust, smoke, clothing, and some building materials, making them suitable for a variety of applications. Cameras developed for commercial markets have focused mainly on security screening ("virtual frisking") and cover many market segments such as security at police stations, prisons, courts, embassies, transportation terminals, as well as anti-theft [1–3]. Cameras for military markets have tended to focus on all-weather navigation [4,5], and especially on rotorcraft brownout for landing in dusty or snowy areas [6]. Millimeter wave radiometers have been used extensively for remote atmospheric sensing and radio astronomy, but these niche markets typically require more sophisticated and expensive sensors that utilize techniques such as Dicke switching and cryogenic cooling to achieve thermal resolution of a few milliKelvin. In contrast, radiometers that address commercial markets must be as simple and inexpensive as possible while providing thermal resolution in the 0.3–0.5 K range. Such radiometers often rely solely on signal processing schemes to improve image quality, for example by detecting and correcting artifacts caused by random drift of the radiometer outputs [7].

The choice of operating frequency depends on the desired trades between device performance, spatial resolution, cost, size/weight, and atmospheric absorption. Although much initial work in the 1990s focused on 35 GHz, the desire to improve spatial resolution coupled with improvements in millimeter wave device technology allowed for operation at W band (75–110 GHz) to take advantage of the broad atmospheric window centered around 94 GHz. As semiconductor device performance continues to improve, groups will likely continue to increase the operating frequency to higher absorption windows, such as 140, 220, or 320 GHz to further improve spatial resolution and/or decrease size/weight [8,9].

0003-6935/10/1900E7-06$15.00/0

Millimeter wave imaging systems may be divided into two distinct classes: "active" systems that require coherent illumination of the scene, and "passive" systems that rely on emission and reflection of incoherent radiation. Each type of system has advantages and disadvantages that must be carefully weighed for the application at hand. Active systems typically have higher sensitivity, are capable of providing range information, and may have a flat form factor. However, active illumination at long wavelengths, whether coherent or incoherent, produces regions of spectral reflection from flat surfaces ("glint") that result in splotchy images whose details are often difficult to discern. Passive systems often rely solely on distributed ambient illumination and therefore suffer less from glint, producing images that users generally find more acceptable and are more amenable to automatic threat or anomaly detection algorithms. In addition, passive systems are covert, which may be desirable in some military applications. However, passive systems inherently do not provide range information and have limited sensitivity.

2. Direct Detection Millimeter Wave Imaging Sensors

In this paper we will describe HRL's development of W band sensors for passive millimeter wave imaging. Our approach has been to keep the millimeter wave portion of the sensor as simple as possible to minimize cost, while providing at least the minimum performance required by camera developers. We utilize a total power radiometer, as indicated in Fig. 1, consisting of an antenna to collect blackbody energy, a low noise amplifier (LNA) to boost the signal, and a square law detector to provide an output voltage proportional to the amplified noise power. The average detected output voltage (not including any detector bias voltage) depends on the effective noise temperature $T_s\,(K)$ received by the antenna, the pre-LNA dissipation factor α (a number between zero and one), the LNA gain G and noise factor F (which becomes the noise figure when expressed in dB), the detector responsivity $\beta\,(V/W)$, and the radiometric RF bandwidth Δf (Hz), as

$$V = k(\alpha(T_s - T_o) + FT_o)G\beta\Delta f, \tag{1}$$

where T_o is the reference temperature for the noise factor and is assumed to be the physical temperature of the detector. The random fluctuations of this voltage have a one-sided power spectral density (PSD, V^2/Hz) equal to [10]

$$S(f) = V^2\left(\frac{2}{\Delta f} + \frac{S_d}{V^2} + \frac{K}{f}\right). \tag{2}$$

The first two terms are, respectively, white noise contributions from downconverted RF noise and detector thermal (and possibly shot) noise, and the third term is $1/f$ (flicker) noise resulting from temporal fluctuations of the LNA gain and detector responsivity.

To form an image, one typically utilizes optics to project radiant energy from a scene onto a focal plane where an array of sensors collects the energy, similar to an IR or visible camera. However, due to the expense of RF components, millimeter wave cameras typically utilize a small array of sensors that is mechanically scanned across the focal plane. Efforts to develop two dimensional focal planes of high sensitivity, low cost, room temperature sensors without LNAs produced significant improvements to detector sensitivity but still fall short of achieving the video-rate sensitivity needed for most imaging applications [11,12]. As the sensors are swept across the focal plane in a scanning system over a "frame" period T_{frame}, each sensor output is averaged over an "integration time" T_{int} to form an image pixel, so that each frame consists of $N = T_{\mathrm{frame}}/T_{\mathrm{int}}$ pixels. One may use Eq. (2) to compute the mean square fluctuation about the average for a set of N such pixels:

$$\langle \Delta V^2 \rangle = V^2\left(\frac{1}{\Delta f\, T_{\mathrm{int}}} + \frac{S_d}{2V^2 T_{\mathrm{int}}} + K \times \ln N\right). \tag{3}$$

The radiometer figure of merit is the thermal resolution, or noise equivalent temperature difference (NETD), equal to the ratio of RMS voltage fluctuation to thermal sensitivity:

$$\begin{aligned}\mathrm{NETD} &= \frac{\sqrt{\langle \Delta V^2 \rangle}}{\mathrm{d}V/\mathrm{d}T_s} \\ &= T_{\mathrm{sys}}\sqrt{\frac{1}{\Delta f\, T_{\mathrm{int}}} + \frac{S_d}{2V^2 T_{\mathrm{int}}} + K \times \ln N},\end{aligned} \tag{4}$$

where $T_{\mathrm{sys}} = V/(\mathrm{d}V/\mathrm{d}T_s) = T_o F/\alpha$ is called the equivalent input system noise temperature and is often expressed as the sum of the receiver noise temperature and input noise temperature: $T_{\mathrm{sys}} = T_{\mathrm{rec}} + T_{\mathrm{ant}}$ [13]. Note that this expression for NETD includes the effects of $1/f$ noise, something that is not normally done for IR sensors. Millimeter wave sensor arrays for commercial applications generally do not use optical choppers due to the size and expense associated with chopping an entire array of sensors. Dicke switches, noise injection, or other means of reducing the effects of $1/f$ noise and drift are also typically cost prohibitive. Instead, the effects of $1/f$ noise are minimized by properly engineering

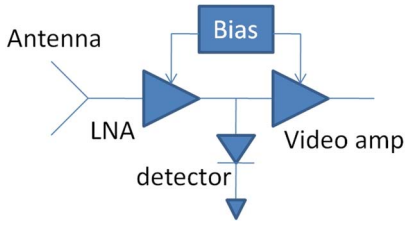

Fig. 1. (Color online) Block diagram of radiometer. Simplicity is key to achieving low cost.

the LNA and detector, and drift is compensated for using software techniques [7].

3. Sb-Based Zero-Bias Detector Monolithic Microwave Integrated Circuits

Prior to these last few years, millimeter wave (mmW) sensors typically utilized biased Schottky diodes for square law detection due to their ease of fabrication, high responsivity, and low junction capacitance. The bias current in a Schottky diode significantly increases detector noise by introducing shot noise and increasing $1/f$ noise. Radiometer front ends typically contained multiple amplifier monolithic microwave integrated circuits (MMICs) with over 50 dB of total gain [14] in order to boost the input signal well above the detector noise level. Utilizing zero-bias detectors reduces detector noise, requiring less gain in the LNA stages. By engineering the detector to be sufficiently responsive while operating at zero bias, one may significantly reduce the front end cost.

Zero-bias detectors have become more widely available in recent years. Planar doped barrier diodes perform well at millimeter wave frequencies, but their sensitivity to growth conditions makes them expensive to manufacture in large quantities. Low barrier Schottky diodes provide good millimeter wave performance and are commercially available for a variety of frequency bands [15]. Although these devices offer high responsivity and relatively low noise, Schottky diode characteristics are inherently temperature sensitive, so they may require additional compensation when used in systems that experience temperature fluctuations.

HRL's development of the zero-bais Sb-based backward tunnel diode [16] resulted in detectors with high responsivity and insensitivity to temperature, with low $1/f$ and no shot noise. The principle of Sb-heterstructure backward diode operation is similar to that of an Esaki backward tunnel diode in that the current controlling mechanism is interband (valence-conduction) tunneling between adjacent energetically offset semiconductor regions. The Esaki diode accomplishes this with a very heavily doped p-n junction. The Sb-heterostructure diode is similar but with the advantage that it has a built-in type II bandgap lineup between InAs and GaAlSb, i.e., the conduction band minimum of InAs intrinsically lies energetically below the valence band maximum of GaSb, as seen in Fig. 2. The consequence is a natural asymmetry in the current flow with bias direction. This results in the attractive feature of these devices, namely, a high nonlinearity in the current–voltage characteristic that produces square-law rectification at zero bias. Another advantage of this diode structure is that the AlSb tunnel barrier width can be chosen to control the junction resistance without significantly affecting the capacitance or current–voltage nonlinearity. And because the current flow near zero bias is based on tunneling and not thermal excitation, the device characteristics are much more stable with temperature than a Schottky device [17].

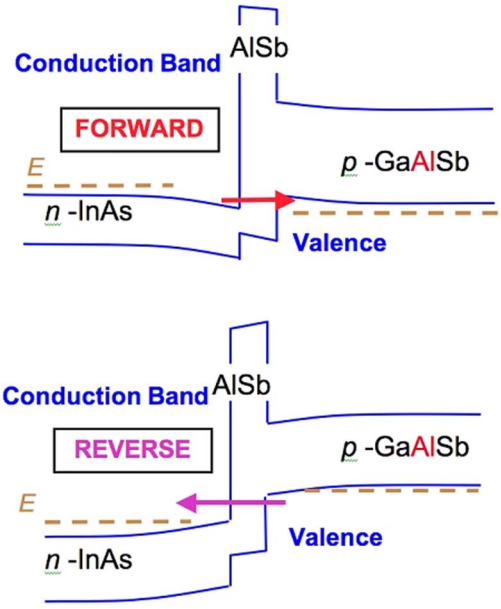

Fig. 2. (Color online) Energy band diagram of the Sb-based backward tunnel diode.

The backward tunnel diode was utilized in a MMIC to provide impedance matched detection at W band, a photograph of which is shown in Fig. 3(a). The circuit consists of an input matching network, series detector, and RF shunt capacitor at the output. A DC return on the input side allows for a single ended output with ground reference. A typical W band detector circuit utilizes a $1\,\mu m^2$ diode, resulting in a junction capacitance of 15 fF, a junction resistance of 800 Ω, and series resistance of about 20 Ω. The curvature coefficient (the ratio of the second derivative to the first derivative of the detector I–V curve at zero volts) is about 32 A/W. Figure 3(b) shows a plot of the typical RF performance of a detector MMIC.

Although these detectors introduce less added noise to the radiometer output than biased detectors, their added noise is not negligible. Detector thermal noise can be calculated directly from the diode resistance, and sufficient LNA gain (typically 25–30 dB) is introduced so that the downconverted RF noise overcomes the thermal noise level. Radiometers that do not utilize a Dicke switch, optical chopper, or some other method of periodic recalibration have performance that is primarily limited by detector $1/f$ noise when operated with integration times longer than a millisecond or so. The $1/f$ noise results from the bias voltage (the detector output is typically sensed as a voltage amplified by a high input impedance amplifier; instead, one may sense detector current fed to a low impedance amplifier, but either approach suffers $1/f$ noise due to induced bias) developed across the detector as a result of rectification of the LNA output noise power. Because the PSD of the $1/f$ noise process is proportional to the square of the detector voltage, the $1/f$ contribution to NETD cannot be mitigated by increasing (or decreasing) LNA gain

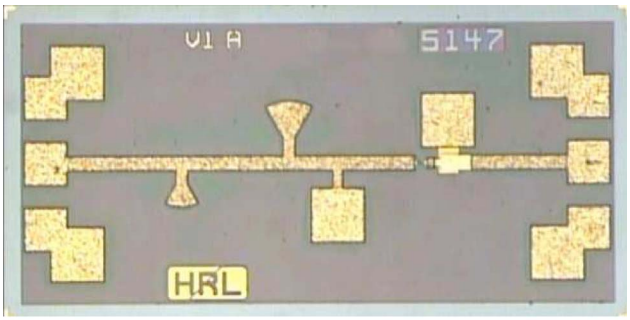

(a)

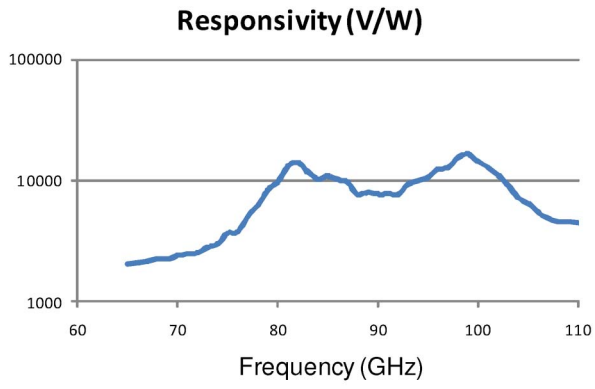

(b)

Fig. 3. (Color online) (a) Photograph of the backward tunnel diode detector MMIC. (b) Plot of measured responsivity.

[see Eq. (4)]. Furthermore, because the $1/f$ noise is generated within the detector itself, as opposed to the video electronics, one may not utilize baseband switching techniques such as correlated double sampling that is used so effectively in IR readout circuitry. The most effective way to correct for the $1/f$ noise within the detector is to modulate the RF input and synchronously detect, but this process adds significant expense and complexity to the receiver and is generally avoided in commercial systems.

4. InP HEMT Low Noise Amplifier, Monolithic Microwave Integrated Circuits

In the 1990s HRL developed an InP high electron mobility transistor (HEMT) LNA process for high performance communication systems that was later leveraged for W band imaging sensors [18]. Figure 4(a) shows a photograph of a five stage LNA and Fig. 4(b) shows a plot of the gain versus frequency. InP HEMT devices offer the lowest noise figure available in any device technology, with LNA noise figures less than 3 dB readily achievable for 94 GHz, room temperature, wideband amplifiers. Recent advances in InP HEMT technology continue to improve circuit performance [19], although state of the art device technologies generally have limited commercial availability. GaAs LNAs cost considerably less than InP due to higher foundry volumes, but the noise figure of GaAs based LNAs is 2–3 dB higher than for InP, directly affecting sensitivity. In addition, the gain per stage of GaAs LNAs is lower

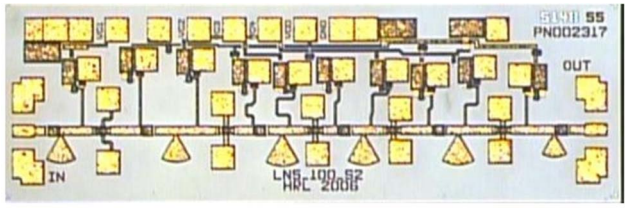

(a)

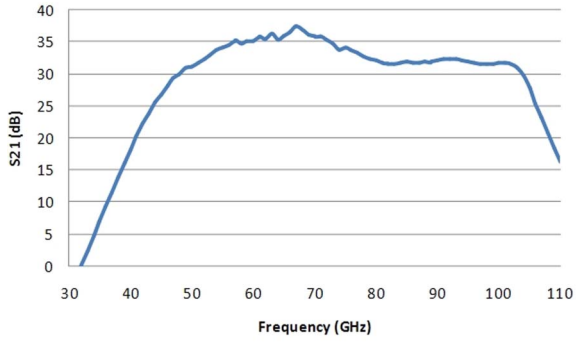

(b)

Fig. 4. (Color online) (a) Photograph of five stage LNA MMIC. (b) Plot of gain versus frequency.

than InP requiring more stages, and possibly multiple MMICs, to achieve the necessary 25–30 dB gain.

Although LNA noise figure has the biggest effect on radiometer performance, gain drift is also significant and must be compensated for in any imaging system. Long term gain drift occurs in all devices and may be dealt with using either hardware- or software-based techniques. Because $1/f$ noise is due to temporal gain fluctuations, hardware techniques to reduce $1/f$ noise can also be used to mitigate steady gain drift, and include Dicke switching and optical chopping. Radiometers that do not utilize such hardware compensation must use some other technique such as long term averaging to detect and compensate for drift. All systems require periodic recalibration by providing known thermal sources to all of the sensors, and the system designer must determine the acceptable rate of calibration for a given application. Note that our NETD expression (4) assumes such a calibration occurs at the end of each frame period.

Because the sensors must detect minute changes in scene temperature, small changes in gain create substantial errors in temperature estimates. LNA gain is generally the dominant radiometer drift mechanism. Using Eq. (1) we see that changes in scene temperature δT_s and LNA gain δG produce a fractional change in output voltage equal to $\delta V/V = \delta T_s/T_{\text{sys}} + \delta G/G$. With a typical system temperature of 700 K and a desired minimum detectable temperature fluctuation of 0.5 K, we see that the gain stability must be much better than about 700 ppm, or 0.003 dB. It does not take long for a typical HEMT to drift outside this range. For example, Fig. 5 shows a plot of normalized radiometer output voltage versus time. Drift is fastest immediately after powering

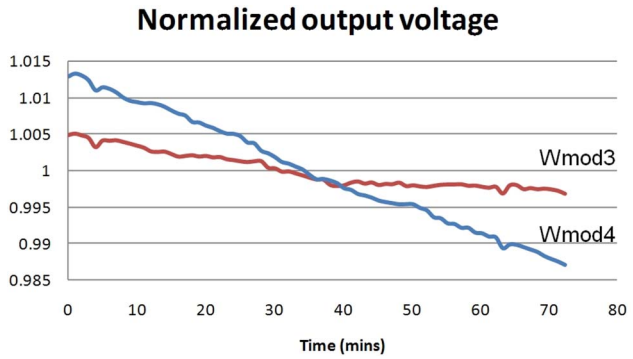

Fig. 5. (Color online) Plot of normalized output voltage versus time for two different sensors. The variation is due to drift in LNA gain. The data were taken following an approximately 15 min. warm up time.

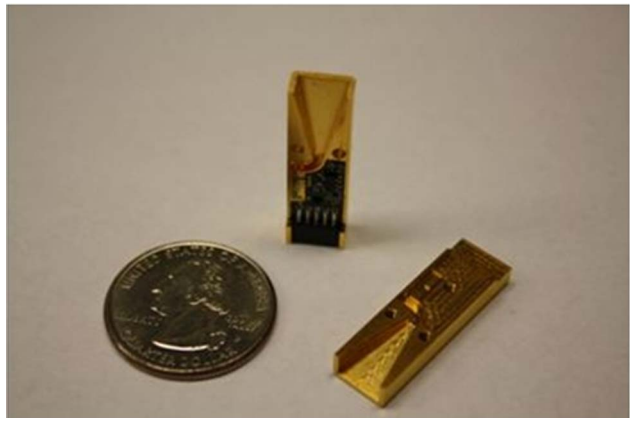

Fig. 6. (Color online) Photograph of a W band imaging sensor from Brijot Imaging Systems.

on the LNA and follows a simple power relation over long time periods. The exponent of the power relation varies randomly from device to device—even in sign, with some gains increasing over time and others decreasing.

5. *W* Band Sensors

A cost competitive millimeter wave imaging system requires reasonably priced sensors that provide the necessary performance. Sensor cost and performance both depend critically on assembly processes. Recent experiences have shown that the manufacturing tolerances of today's standard automated assembly processes provide acceptable performance and repeatability for W band sensors. The need for only two MMICs within the sensor together with standard automated assembly techniques allows one to achieve high sensor performance while continuing to drive down costs as sales volumes increase.

Integrating the LNA and detector MMICs together with an antenna and video electronics is reasonably straightforward. Horn antennas provide excellent overall efficiency (low dissipation and high beam efficiency), and simple E-plane probes on alumina substrates transition the fields from waveguide to microstrip with losses typically between 0.5 and 1 dB. An electronic printed circuit board is often included within the sensor module to provide video amplification and possibly LNA bias. Figure 6 shows an example of such a module, developed by Brijot Imaging Systems.

Substantial module characterization can be accomplished using low frequency measurements of the sensor output. Recording the output voltage while the antenna is directed at RF absorbing material that is sequentially held at two known temperatures (e.g., room temperature and 77 K) allows us to compute the thermal sensitivity dV/dT_s and the system noise temperature $T_{\text{sys}} = V/(dV/dT_s)$. Assuming we know the front end dissipation factor α, we may use Eq. (1) at the two temperatures to compute the noise factor F and the gain–bandwidth product $G\beta\Delta f$. We may estimate the RF bandwidth from the output voltage PSD as follows. With the antenna directed at room temperature absorber we measure the output spectrum and estimate the white and $1/f$ noise PSD levels by curve fitting. Repeating the measurement and curve fitting with the LNA biased off provides a direct measurement of detector white noise. The RF radiometric bandwidth may be computed from the difference between the "on" and "off" white noise PSD levels using Eq. (2):

$$\Delta f = \frac{2V^2}{S|_{\substack{\text{white,}\\ \text{LNA on}}} - S|_{\substack{\text{white,}\\ \text{LNA off}}}}. \tag{5}$$

The $1/f$ K factor may be determined directly from the spectrum curve fit. Finally, NETD may be estimated from the frequency domain data using Eq. (4). When the frequency exponent of the $1/f$ noise PSD differs from unity, as is often the case in practice, Ref. [10] shows how to properly normalize the K factor so that (4) can be used directly.

As examples of sensor performance, Table 1 shows measured results from five different imaging sensors that were designed and assembled at HRL and characterized using the above methods. The chipsets

Table 1. Measured Performance and Extracted Parameters

V, mV	dV/dT, uV/K	$K(1/f$ const)	$G\beta$, V/uW	NF, dB	BW, GHz	NETD, K
1.4	1.8	3.3	4.5	4.4	28	0.29
5.3	7.0	13	14	4.2	35	0.52
5.8	6.9	6.1	20	4.6	23	0.41
0.6	0.52	10	1.1	5.9	33	0.69
3	4.3	5.3	12	3.8	26	0.32

were selected for specific experiments, so the results do not necessarily reflect typical performance one would expect from chipsets selected at random. The listed output voltage is prior to video amplification, and the K factors were normalized to compensate for nonunity $1/f$ frequency exponents. The NETD calculations assume an integration time of 3.125 ms for $N = 32$ integration periods.

6. Future Efforts

As millimeter wave device performance continues to improve, new devices will be incorporated into MMIC circuits for future generations of imaging chipsets. Next generation InP HEMT devices will improve radiometer sensitivity by reducing noise figure, and the increased gain per stage will result in smaller, cheaper MMICs at *W* band. In addition, these devices will enable radiometer operation above *W* band (e.g., 220 or 320 GHz), improving spatial resolution and/or reducing camera size. These next generation sensors will provide new levels of performance that will in turn help stimulate sales in this small but growing market.

References

1. G. V. Tryon, "Millimeter wave case study of operational deployments: retail, airport, military, courthouse, and customs," Proc. SPIE **6948**, 694802 (2008).
2. T. D. Williams and N. M. Vaidya, "A compact, low cost, passive mmW security scanner," Proc. SPIE **5789**, 109–116 (2005).
3. C. A. Martin, "Rapid passive mmW security screening portal," Proc. SPIE **6948**, 6948J1 (2008).
4. A. H. Lettington, D. Dunn, N. E. Alexander, A. Wabby, B. N. Lyons, R. Doyle, J. Walshe, M. Attia, and I. M. Blankson, "Design and development of a high performance passive millimeter wave imager for aeronautical applications," Proc. SPIE **5410**, 210–218 (2004).
5. R. Appleby, P. Coward, and J. N. Sanders-Reed, "Evaluation of a passive millimeter wave (PMMW) imager for wire detection in degraded visual conditions," Proc. SPIE **7309**, 7309A1 (2009).
6. C. A. Martin and V. G. Kolinko, "Improved passive millimeter wave imaging from a helicopter platform," Proc. SPIE **5409**, 8–14 (2004).
7. A. H. Lettington, Q. H. Hong, and D. G. Gleed, "Removing line patterns from infrared and passive millimeter wave images," Proc. SPIE **2298**, 24–29 (1994).
8. C. Mann, "First demonstration of a vehicle mounted 250 GHz real time passive imager," Proc. SPIE **7311**, 7311Q1 (2009).
9. D. L. McMakin, D. M. Sheen, H. D. Collins, T. E. Hall, and R. H. Severtsen, "Wideband millimeter wave holographic surveillance systems," Proc. SPIE **2511**, 131–142 (1995),
10. J. J. Lynch, H. P. Moyer, J. H. Schaffner, Y. Royter, M. Sokolich, B. Hughes, Y. J. Yoon, and J. N. Schulman, "Passive millimeter-wave imaging module with preamplified zero-bias detection," IEEE Trans. Microwave Theory Tech. **56**, 1592–1600 (2008).
11. J. H. Schaffner, J. J. Lynch, K. V. Guinn, J. N. Schulman, H. P. Moyer, R. Bowen, and M. Musni, "A wideband radiometer module for an unamplified direct detection scalable *W*-band imaging arrays," Proc. SPIE **6948**, 694807 (2008).
12. H. Kazemi, C. Nguyen, B. Brar, G. Rebeiz, G. Nagy, L. Tran, A. Young, and E. R. Brown, "Low cost modular integrated horn antenna array using heterojunction barrier diode detectors," paper presented the International Microwave Symposium of the IEEE Microwave Theory and Techniques Society, Atlanta, Georgia, USA, 10–15 June 2008.
13. M. Tiuri, "Radio astronomy receivers," IEEE Trans. Antennas Propag. **12**, 930–938 (1964).
14. R. Appleby, R. N. Anderton, S. Price, N. A. Salmon, G. N. Sinclair, J. R. Borrill, P. R. Coward, P. Papakosta, A. H. Lettington, and D. A. Robertson, "Compact real time (video rate) passive millimeter wave imager," Proc. SPIE **3703**, 13–20 (1999).
15. J. L. Hesler and T. W. Crowe, "Responsivity and noise measurements of zero-bias Schottky detectors," paper presented at the 18th International Symposium on Space Terahertz Technology, Pasadena, California, USA, March 2007.
16. J. N. Schulman and D. H. Chow, "Sb-heterostructure interband backward diodes," IEEE Electron. Device Lett. **21**, 353–355 (2000).
17. N. Su, Z. Zhang, J. N. Schulman, and P. Fay, "Temperature dependence of high frequency and noise performance of Sb-heterostructure millimeter wave detectors," IEEE Electron. Device Lett. **28**, 336–339 (2007).
18. M. G. Case, C. Pobanz, S. Weinreb, M. Matloubian, M. Hu, M. Wetzel, P. Janke, and C. Ngo, "Low cost, high performance *W* band LNA MMICs for millimeter wave imaging," Proc. SPIE **4032**, 89–96 (2000).
19. X. B. Mei, C. H. Lin, L. J. Lee, Y. M. Kim, P. H. Liu, M. Lange, A. Cavus, R. To, M. Nishimoto, and R. Lai, "A *W* band InGaAs/InAlAs/InP HEMT low noise amplifier MMIC with 2.5 dB noise figure and 9.4 dB gain at 94 GHz," paper presented at the 2008 IEEE 20th Conference on Indium Phosphide and Related Materials (IPRM'08), Versailles, France, 25–29 May 2008.